Atmos. Chem. Phys. Discuss., 13, 30013–30037, 2013
www.atmos-chem-phys-discuss.net/13/30013/2013/
doi:10.5194/acpd-13-30013-2013

Atmospheric Chemistry and Physics Discussions

On the link between the Amazonian forest properties and shallow cumulus cloud fields

R. H. Heiblum[1], I. Koren[1], and G. Feingold[2]

[1]Department of Environmental Sciences and Energy Research, Weizmann Institute, Rehovot 76100, Israel
[2]NOAA Earth System Research Laboratory (ESRL), Chemical Sciences Division, Boulder, Colorado 80305, USA

Received: 15 October 2013 – Accepted: 1 November 2013 – Published: 15 November 2013

Correspondence to: I. Koren (ilan.koren@weizmann.ac.il)

Published by Copernicus Publications on behalf of the European Geosciences Union.

Abstract

During the dry season the Amazon forest is frequently covered by shallow cumulus clouds fields, referred to here as Forest Cumulus (FCu). These clouds are shown to be sensitive to landcover and exhibit a high level of spatial organization. In this study we use satellite data to perform a morphological classification and examine the link between FCu cloud field occurrence and the Enhanced Vegetation Index (EVI), which is commonly used as a measure for forest density and productivity. Although secondary to the higher order effects of meteorology and biomass burning, a clear positive linear relation between EVI (i.e. surface properties) and FCu field occurrence is seen over forest landcover, implying a strong coupling between forest surface fluxes and the cloud organization above. Over non-forest landcover the relation between EVI and FCu occurrence is non-linear, showing a reduction of FCu for high EVI values. We find that forest to non-forest transition zones display a superposition of the two different landcover dependencies.

1 Introduction

During the Amazon dry season (austral winter months, June–September), the ITCZ moves northward (reaches $\sim 10^{\circ}$ N at mid August) and is replaced by South Atlantic Subtropical High (SASH) (Nobre et al., 1998). During this period, large scale subsidence dominates the region and relatively stable meteorological conditions prevail. Under these conditions, organized fields of shallow cumulus (Cu) clouds form over and near the forest during the daytime hours when surface triggered convection is possible and the humidity near the canopy is high enough. The formation of these clouds has a clear diurnal cycle with a maximum in their formation during the afternoons.

A typical image of these cloud fields can be seen in Fig. 1, taken at 1 September, 13:30 local time. The clouds form almost exclusively over land areas; i.e. clouds are absent above the Amazon River and its tributaries. One of the noticeable, although not

ACPD
13, 30013–30037, 2013

exclusive, properties of these clouds is their tendency to organize in linear patterns parallel to the wind direction (Fig. 2). They can often be considered analogous to cloud streets (Ramos da Silva et al., 2011), which are typically observed during cold air outbreaks over warmer oceanic waters (Brümmer, 1999). In this work these cloud fields are shown to be very sensitive to changes in the environmental conditions and therefore they can serve as a "litmus test" for any action that may change the conditions in which they form. They are hereafter referred to as Forest Cumulus (FCu) fields (more details on the FCu are given in Sect. 2). Daytime FCu cloud fields similar to those seen in Figs. 1 and 2 can be observed in several other locations around the globe such as central Africa during most of the year, or northeast America and Siberia during the boreal summer. The common denominator in all cases is their preferred formation over dense, large-scale forests during stable meteorological conditions, when formation of more developed clouds is suppressed.

Landcover change effects on clouds can be divided by temporal and spatial scales into short (immediate) or long term effects, or local to global spatial scales (Pielke Sr. et al., 2011); here we will focus on the short term ones. The immediate effects of landcover changes are attributed to changes in the surface radiation budget (Betts, 2009). Different landcover types exhibit different albedo, surface roughness, moisture content, etc. (Bastable et al., 1993). Such changes affect the energy fluxes to the atmosphere, the partition of this energy to sensible and latent heat, and the turbulent transfer of those fluxes to the atmosphere. Eventually, these changes influence the diurnal evolution of the atmospheric boundary layer (Betts, 2000). Deforested areas in the Amazon (either pasture or cropland) usually display higher sensible heat and lower latent heat fluxes in comparison with the forested areas, which in turn can enhance the growth of the boundary layer during the day and favor the formation of larger convective clouds (Fisch et al., 2004). Moreover, surface heterogeneities often result in local mesoscale breezes which can also affect low-level convergence patterns and cloud formation (Rabin et al., 1990; Souza et al., 2000).

ACPD
13, 30013–30037, 2013

Generally there exists a preference for shallow Cu formation over densely forested areas rather than savanna and pasture (located around the southern boundaries of the Amazon basin) (Cutrim et al., 1995). Nevertheless, most observational studies, including those listed above, have focused exclusively on deforested pockets within forested areas, emphasizing the importance of mesoscale circulations driven by landcover transitions rather than more subtle changes within a landcover type.

They have shown a clear preference for shallow Cu formation over deforested areas (Cutrim et al., 1995; Chagnon et al., 2004; Wang et al., 2009), and for deep convective cloud formation over the surrounding forested areas (Wang et al., 2009). Additionally, transition zones between landcover types have been shown to display strong precipitation gradients, with a maximum precipitation on the deforested side but close to the forest (Knox et al., 2011). These results however, are confined mainly to the southwest regions of the Amazon, which are highly deforested and experience very stable meteorological conditions during the dry season. Moreover, studies in other regions of the world such as southwest Australia (Ray et al., 2003) and Costa-Rica (Nair et al., 2003) show a preference for shallow cumulus formation over native vegetation and forested areas rather than adjacent deforested areas.

Much of the Amazon deforestation is a result of massive biomass burning events which occur during the dry season (Koren et al., 2004). Biomass burning emits high concentrations of absorbing aerosols to the atmosphere, which can interact with radiation (i.e. scattering and absorbing of shortwave and longwave radiation) and affect the temperature profile and therefore static stability, or serve as Cloud Condensation Nuclei (CCN) and affect the microphysical processes and evolution of clouds and precipitation (Koren et al., 2008). Hence, it is essential to address aerosols and decouple their effects on clouds from the landcover change effects on clouds.

The goal of this work is to evaluate the morphological characteristics of the Amazon FCu fields, and to use a statistical approach to study the effects of landcover change on the FCu fields over the Amazon region. Specifically we use the EVI (Enhanced Vegetation Index) as a measure of the wellbeing of the forest. It has been shown that

ACPD
13, 30013–30037, 2013

this index correlates well with forest productivity and canopy density, and can be a good predictor for evapotranspiration and moisture fluxes to the lower atmosphere, which in turn drive the formation of Amazonian clouds.

2 Methods

In this study we combine raw satellite data in the visible for cloud morphology and Aerosol Optical Depth (AOD) analyses, landcover information and vegetation indices for surface characterization, and reanalysis data for specification of the meteorological conditions. True color data at 0.5 km resolution, AOD data at 1° resolution, and land surface properties derived from the MODerate resolution Imaging Spectroradiometer (MODIS) onboard the Aqua satellite are used (Salomonson et al., 1989; Friedl et al., 2010; Running et al., 1994; Remer et al., 2005). The Aqua overpass is at 13:30 LST, at the time when energy fluxes from the surface are maximum (Fisch et al., 1996) and the FCu fields over the Amazon are already established. The study region of interest is seen in Fig. 1, and spans from 58.54° W, 5.69° N (northwest corner) to 49.45° W, 13.19° S (southeast corner), an area of 2100 km × 950 km. The topography of the study region is low, and devoid of large gradients except some patches in the northern part, and a gradual rise to higher topography in the southern part. Analyses of topographical effects on the FCu fields showed no clear correlations. Therefore, we exclude analyses of topography effects in this work. Data were collected for the dry season months, July–August–September (J-A-S) during both 2010 and 2011.

When shifting the analysis from cloud to cloud-field properties, the nature of the analysis shifts from deterministic to statistic. Therefore we are interested in the statistical properties of the spatial distributions of the cloud fields as opposed to the average properties of specific clouds. Unlike the MODIS operational cloud masks that need either to avoid cloud contamination of the cloud-free atmosphere (Martins et al., 2002), or in the case of cloud retrievals to make sure that the cloud mask is free of non cloudy pixels (Ackerman et al., 1998), in this work we designed spatial operators and filters

ACPD
13, 30013–30037, 2013

that are sensitive to the spatial characteristics of the organized FCu fields. Our algorithm (summarized in Fig. 3) is tuned to calculations of statistical parameters of the field.

The first stage of processing is a construction of a basic cloud mask, achieved by applying a threshold (> 0.58) to the reflectance of the RGB channels (bands 1, 3, 4, respectively). Unlike clouds, most bright pixels that are not clouds (e.g. bright roads or sand patches) are not white (e.g. have spectral dependence in the visible spectrum) therefore another threshold (< 0.08) is applied to the absolute differences in the reflectance between the red and blue. The morphological characteristics of the cloud field were calculated for a moving window of 51×51 pixels (25.5 km $\times$ 25.5 km). Five basic characteristics where shown to contain most of the information: cloud fraction, mean and standard deviation of distances between cloud centroids, and mean and standard deviation of cloud areas.

Based on the above criteria we classified the cloud fields into three classes: FCu, deeper convective clouds and sparse to no-clouds (see Table 1). The classification was tuned and validated visually using data from 100 s of boxes of cloud fields (see Fig. 3c). The boxes were used to calculate the mean statistics of the FCu clouds fields. The typical FCu field has a cloud fraction of 0.24 ± 0.02, mean cloud area of 3.13 ± 0.37 km^2, mean standard deviation of cloud area of 5.64 ± 1 km^2, mean distance between cloud centroids of 2.31 ± 0.31 km, and mean standard deviation of distances between cloud centroids of 0.87 ± 0.07 km. The narrow distribution of these key cloud properties allowed for a robust detection of the fields.

After performing the analysis above for all days during J-A-S (a total of 75–80 overpasses), the probability for an FCu field (hereafter named pFCu) to exist was calculated for each pixel (see Fig. 3d). Similar methodologies have been used in other studies of shallow cumulus clouds (Ray et al., 2003; Cutrim et al., 1995). It is important to note that the classification results where shown to be robust and not sensitive to small variations in the selected thresholds.

ACPD
13, 30013–30037, 2013

Yearly classification of different landcover types was done using the MODIS collection 5 MCD12Q1 product (Friedl et al., 2010). The product includes five types of landcover classifications, out of which the 14-class University of Maryland (UMD) classification was chosen (Hansen et al., 2000). For the purposes of this study, we divided the UMD landcover classification into three types: (i) Forest, classes 1 through 5, (ii) Non-Forest, classes 6 through 16, and (iii) Water, class 17.

Spectral definitions for MODIS vegetation indices (NDVI and EVI) and their validations over numerous sites can be found in previous papers (Huete et al., 2002; Mu et al., 2007). Both vegetation indices can be used to assess the surface energy budget (latent heat, Bowen ratio) components and plant physiology components such as evapotranspiration, leaf area index, fractional vegetation cover, canopy architecture and more (Glenn et al., 2008). Since NDVI tends to saturate in areas of high biomass (Huete et al., 2002), EVI is preferred in our study. Furthermore, studies have shown EVI to be better correlated with evapotranspiration than NDVI, with linear correlation coefficients (r^2) usually ranging between 0.7 and 0.9 (Glenn et al., 2010; Nagler et al., 2005). Henceforth we shall use EVI as a general measure of vegetation density and productivity over the forest and non-forest landcovers.

Focusing on the southern half of the domain, Fig. 3d clearly shows reduction in the probability for FCu fields. The same pattern exists for the year 2010. Using NOAA-NCEP Global Data Assimilation System (GDAS) reanalysis data (Saha et al., 2006; Parrish and Derber, 1992), we examined the spatial patterns of various meteorological parameters (J-A-S averages). The two parameters that were found to best reflect the spatial variance of the FCu fields are the Geopotential Height (HGT) at 700 hPa (see Fig. 4a) and the Relative Humidity (RH) at 850 hPa (see Fig. 4b).

ACPD
13, 30013–30037, 2013

3 Results

3.1 Forest Cumulus (FCu) dependence on meteorology

The meteorological context of the FCu probability is shown in Fig. 4c and d. The north-south pFCu differences over the land are best captured by the Geopotential Height (HGT) at 700 hPa field. The value of HGT = 3157 m (indicated by the dashed line in Fig. 4a and solid line in Fig. 4c) was chosen as the boundary between the northern part of the Amazon region (NA in Fig. 4a and c) that shows little meteorological variance and the southern part of the Amazon region (SA in Fig. 4a and c) that shows high coupling between pFCu and meteorology. To minimize meteorological influence, only the northern region (NA) is used to test large-scale vegetation index effects on FCu fields.

Patterns of RH at 850 hPa may affect some of the features seen in Fig. 3d as well. The east to west positive gradient in the southern Amazon (SA) pFCu seems to correspond to the east-west RH gradient seen in Fig. 4b. Additionally, from the dependence of pFCu on RH in Fig. 4d we can see that areas with high RH (RH > 80 %, indicated by the dashed line in Fig. 4b) are less favorable for FCu formation. The high RH areas are mainly coastal regions, and the reduction in pFCu there is probably due to increased cloud activity (i.e. the cloud fraction (CF) and mean area (σ_A) in coastal areas is frequently above the upper thresholds in Table 1) as a result of mesoscale coastal breezes observed in many previous works (Heiblum et al., 2011; Malda et al., 2007). It should be noted that large scale pFCu dependence on meteorology is similar for both forest and non-forest landcover types.

3.2 Bi-yearly comparison of cloud fields and AOD

The average aerosol optical depth (AOD) together with the cloud field detection algorithm results are summarized in Fig. 5. A striking difference in AOD between 2010 and 2011 can be seen, with average values reaching above 0.8 in the southwest part of the

ACPD
13, 30013–30037, 2013

region during 2010 but limited to 0.25 during 2011. Moreover, the spatial variance of AOD is much smaller during 2011 and is unlikely to be a major factor in pFCu variability. The high AOD during 2010 can be explained by both the extreme drought (Lewis et al., 2011) and frequent fires (Ten Hoeve et al., 2012) (i.e. abundance of biomass burning aerosol) in the Amazon basin that year. However, it should be noted that the drought's effect on our study region was minimal compared to the rest of the basin.

Previously discussed cloud features such as FCu field preference over the northern Amazon (NA) region, and preference for deep convective clouds in high RH areas (i.e. coastal areas) are seen. A relatively high chance for deep convective clouds in the northwest part of the study region may be due to variable terrain and complex topography in that region as well (see Fig. 1). Water bodies such as the Amazon River, Atlantic Ocean, and lakes clearly inhibit all types of cloud formation. Although the general patterns of clouds field probabilities are similar in 2010 and 2011, the most significant differences appear to be related to AOD effects. Areas of high AOD (AOD > 0.5, indicated by white dashed contour in Fig. 5) during 2010 correspond to areas of lower pFCu and a higher probability of observing sparse or no-clouds in comparison with 2011. Moreover, the northern border of the high AOD plume acts as a boundary between low and high pFCu values.

The relative difference between pFCu during 2010 and 2011 is shown in Fig. 6. We define the relative difference here as: $\frac{\mathrm{pFCu}_{2011}-\mathrm{pFCu}_{2010}}{\overline{\mathrm{pFCu}}}$, where $\overline{\mathrm{pFCu}}$ is the two year average. A low-pass 60 km radius filter was applied to reduce small-scale variability. Although pFCu was higher throughout the most of the study region in 2011, the largest differences (up to 90 %) are seen in areas of high AOD during 2010, whereas in other the parts of the domain, relative differences are limited to the −15 % to 50 % range.

A comparison of the meteorological parameter averages between years 2010 and 2011 in the high AOD region shows minor differences of less than ±2 m for HGT at 700 hPa and 0–10 % for RH at 850 hPa, suggesting that the lower pFCu during 2010 was due to high AOD and not meteorology.

ACPD
13, 30013–30037, 2013

We may also speculate that the slightly increased occurrence of deep convective activity during 2010 is related to the higher values of AOD that year, possibly indicating invigoration of convective clouds by biomass burning aerosol. For our purposes, we use the 2011 data, which shows more favorable conditions for FCu and is less likely to be affected by smoke.

3.3 Enhanced Vegetation Index (EVI) effect on Forest Cumulus (FCu) fields

To minimize influences of AOD and meteorology on the data, we limit the analysis of EVI effects on FCu fields to the NA region (excluding RH > 80 % areas) during 2011. The pFCu data were sorted as a function of EVI for forest (blue dots) and non-forest (magenta dots) landcovers separately (see Fig. 7a). Bin statistics are included in the figure legend/caption. For the forest landcover, we see a positive dependence of pFCu on EVI. This dependence is especially strong for the lower EVI values. The increase in pFCu then saturates at a moderate value of about EVI = 0.54, and finally shows an additional increase at the high end values of EVI > 0.585. For the non-forest landcover, the dependence of pFCu on EVI is somewhat different. For low EVI values (EVI < 0.35), there is a strong positive dependence (similar to that seen in forest landcover), but for higher values of EVI > 0.35 the dependence can be represented as parabolic, with a peak at EVI = 0.48. It is important to note that for all EVI values, there is a higher chance of observing an FCu field above forest landcover than non-forest landcover.

Even though the data in Fig. 7a can be considered as decoupled from meteorology and AOD, we have not yet considered the effects of mesoscale circulations that may form at the boundaries and transition areas between landcover types. Since these circulations are local, their intensity can be represented by the distance from the landcover boundaries. As seen in Fig. 7b for the NA region, pFCu over forest landcover is lowest close to the boundaries with other landcover types, then increases sharply with large variance at short distances (< 5 km), and is relatively constant at distances larger than ∼ 10 km. The variance seen for distances higher than 80 km may be due to local topography and forest changes. To try and eliminate the mesoscale effects from

ACPD
13, 30013–30037, 2013

the EVI analysis, we divided the data into two subsets: i) Forest data within 10 km of other landcover types (Fig. 7c), which we assume includes the bulk of mesoscale circulation effects and (ii) Forest data further than 10 km away from other landcover types (Fig. 7d), which we consider to be free of mesoscale circulation effects. There was no point in doing the same exercise for non-forest landcover since more than 95 % of that data is closer than 10 km to other landcover types.

Figures 7c and d illustrate how the pFCu dependence on EVI shifts as we penetrate deeper into the forested areas. In Fig. 7c, forest landcover data was divided to 0–1 km, 1–2.5 km, 2.5–5 km, and 5–10 km distance intervals from any other landcover. The non-forest pFCu dependence on EVI from Fig. 7a is added for reference. A gradual transition from a non-forest-like dependence on EVI (i.e. negative parabolic) to a deep-forest-like dependence on EVI (i.e. positive linear, black dashed line in Fig. 7c) is seen. Hence, we can assume that in transition zones between forest landcover and water/non-forest landcovers, a superposition of deep forest and non-forests dependencies on EVI takes place. Generally, for a given EVI value the further the distance from water/non-forest landcovers, the higher the chance of observing FCu fields.

For deep forest data further than 10 km away from other landcover types (blue dots, Fig. 7d) we can see a positive linear dependence of pFCu on EVI. We applied a linear fit to the data ($R^2 = 0.98$, fit details added in figure legend) and obtained a slope of $\frac{\partial(\text{pFCu})}{\partial(\text{EVI})} = 0.14$. Clearly, the well-being and productivity of the deep forest promotes the formation of FCu fields. To test the significance of the linear trend above (Fig. 7d, blue line), we applied two low-pass disk shaped filters to the EVI data, one with a radius of 5 km (green stars and line, Fig. 7d) and the other with a radius of 25 km (red triangles and line, Fig. 7d). Our assumption is that using "smoothed" EVI data, being less sensitive to local noise, reveals the more robust larger-scale effects of EVI on pFCu. The results of this analysis show that indeed the positive linear trend seen for the deep forest is robust, with stronger dependencies as filter size increases. The slope of EVI vs. pFCu increases to $\frac{\partial(\text{pFCu})}{\partial(\text{EVI})} = 0.42$ for the 5 km filter and $\frac{\partial(\text{pFCu})}{\partial(\text{EVI})} = 0.77$ for the 25 km fil-

ACPD
13, 30013–30037, 2013

ter, an increase of 200 %, and 450 %, respectively. For larger filters with radius > 30 km, the main signal decays because of significant loss of EVI spatial information.

4 Discussion and Conclusions

In this work we examine the link between the Amazon forest and the clouds that form above it, as part of the effort towards understanding how the anthropogenic forest dilution may affect clouds. By defining Forest Cumulus (FCu) clouds fields, we have created a simple metric that is clearly tightly coupled and highly sensitive to surface changes in the Amazon region. Although chosen subjectively, we note that results of this work are insensitive to changes in the upper and lower thresholds. We tested several sets of threshold ranges and even though the absolute values of pFCu do change, the trends obtained in Sect. 3.3 were the same.

The bulk of the analyses were concentrated on decoupling lower order effects (such as meteorology and biomass burning) from the more subtle higher order effect of forest EVI. Not surprisingly, the meteorological conditions are the main factor that sets the stage for FCu formation. Although the entire study region experiences stable conditions during the dry season, weak meteorological gradients control where FCu fields can form. The South Amazon (SA) subset is usually too dry and stable to enable FCu formation, above forest and non-forest landcover alike. In contrast, the northwestern part and coastal areas of the North Amazon (NA) subset experience relatively unstable conditions which are realized by the increased presence of deep convective clouds and reduction in pFCu. The results in Figs. 5 and 6 strengthen previous findings that show that high AOD (i.e. high concentrations of biomass burning aerosol) tends to stabilize the atmosphere and inhibit all types of cloud formation; however, in some cases high AOD may result in cloud invigoration (Koren et al., 2008; Andreae et al., 2004; Davidi et al., 2009).

Regarding the link between surface EVI and pFCu, four main conclusions can be drawn:

ACPD
13, 30013–30037, 2013

1. FCu fields form exclusively over land areas in the Amazon region, preferably over forest landcover.

2. The chance of observing FCu fields over forest landcover increases linearly with EVI.

3. The chance of observing FCu fields over non-forest landcover has a negative parabolic dependence on EVI, and is always lower than over forest landcover.

4. The dependence of pFCu on EVI in transition areas from non-forest/water boundaries into forested landcover can be expressed as a superposition of forest and non-forest dependencies.

These findings show the strong control that landcover and landcover gradients exert on FCu. Even though the dependence need not be linear, EVI can be considered highly correlated with evapotranspiration, implying that high latent heat (moisture) fluxes are crucial for the development of the FCu fields. The peculiar decrease in pFCu at high EVI for non-forest landcover that is not seen over the forest may be due to the different water resistances, albedos, Bowen ratios, or even canopy structure between the different landcovers. Hence, these parameters should be explored carefully in future research attempts.

Acknowledgements. This research was supported by the European Research Council under the European Union's Seventh Framework Programme (FP7/2007-2013)/ERC (CAPRI, grant # 306 965) and by NASA Interdisciplinary Science (IDS) project managed by H. Maring. GF was funded by NOAA's Climate Goal. We acknowledge the use of Rapid Response imagery (true color images in the work) from the Land Atmosphere Near-real time Capability for EOS (LANCE) system operated by the NASA/GSFC/Earth Science Data and Information System (ESDIS) with funding provided by NASA/HQ. Aerosol Optical Depth (AOD) data and visualizations (Figs. 5 and 6) were produced with the Giovanni online data system, developed and maintained by the NASA GES DISC.

ACPD
13, 30013–30037, 2013

References

Ackerman, S. A., Strabala, K. I., Menzel, W. P., Frey, R. A., Moeller, C. C., and Gumley, L. E.: Discriminating clear sky from clouds with MODIS, J. Geophys. Res.-Atmos., 103, 32141–32157, doi:10.1029/1998jd200032, 1998.

Amante, C. and Eakins, B. W.: ETOPO1 1 Arc-Minute Global Relief Model: Procedures, Data Sources and Analysis. NOAA Technical Memorandum NESDIS NGDC-24, 19 pp., available at: http://www.ngdc.noaa.gov/mgg/global/relief/ETOPO1/docs/ETOPO1.pdf, March 2009.

Andreae, M. O., Rosenfeld, D., Artaxo, P., Costa, A. A., Frank, G. P., Longo, K. M., and Silva-Dias, M. A.: Smoking rain clouds over the Amazon, Science, 303, 1337–1342, doi:10.1126/science.1092779, 2004.

Bastable, H. G., Shuttleworth, W. J., Dallarosa, R. L. G., Fisch, G., and Nobre, C. A.: Observations of climate, albedo, and surface radiation over cleared and undisturbed Amazonian forest, Int. J. Climatol., 13, 783–796, doi:10.1002/joc.3370130706, 1993.

Betts, A. K.: Idealized model for equilibrium boundary layer over land, J. Hydrometeorol., 1, 507–523, doi:10.1175/1525-7541(2000)001<0507:Imfebl>2.0.Co;2, 2000.

Betts, A. K.: Land–surface–atmosphere coupling in observations and models, J. Adv. Model. Earth Sy., 1, 18, doi:10.3894/James.2009.1.4, 2009.

Brümmer, B.: Roll and cell convection in wintertime arctic cold-air outbreaks, J. Atmos. Sci., 56, 2613–2636, doi:10.1175/1520-0469(1999)056<2613:RACCIW>2.0.CO;2, 1999.

Chagnon, F. J. F., Bras, R. L., and Wang, J.: Climatic shift in patterns of shallow clouds over the Amazon, Geophys. Res. Lett., 31, L24212, doi:10.1029/2004gl021188, 2004.

Cutrim, E., Martin, D. W., and Rabin, R.: Enhancement of Cumulus Clouds over Deforested Lands in Amazonia, B. Am. Meteorol. Soc., 76, 1801–1805, doi:10.1175/1520-0477(1995)076<1801:Eoccod>2.0.Co;2, 1995.

Davidi, A., Koren, I., and Remer, L.: Direct measurements of the effect of biomass burning over the Amazon on the atmospheric temperature profile, Atmos. Chem. Phys., 9, 8211–8221, doi:10.5194/acp-9-8211-2009, 2009.

Fisch, G., Culf, A., and Nobre, L.: Modelling convective boundary layer growth in Rondonia, edited by: Gash, J. H. C., Nobre, C. A., Roberts, J. M., and Victoria, R. L., Amazonian Deforestation and Climate. John Wiley & Sons, Chichester, UK, 425–436, 1996.

ACPD
13, 30013–30037, 2013

Fisch, G., Tota, J., Machado, L. A. T., Dias, M. A. F. S., Lyra, R. F. D., Nobre, C. A., Dolman, A. J., and Gash, J. H. C.: The convective boundary layer over pasture and forest in Amazonia, Theor. Appl. Climatol., 78, 47–59, doi:10.1007/s00704-004-0043-x, 2004.

Friedl, M. A., Sulla-Menashe, D., Tan, B., Schneider, A., Ramankutty, N., Sibley, A., and Huang, X. M.: MODIS Collection 5 global landcover: Algorithm refinements and characterization of new datasets, Remote Sens. Environ., 114, 168–182, doi:10.1016/j.rse.2009.08.016, 2010.

Glenn, E. P., Huete, A. R., Nagler, P. L., and Nelson, S. G.: Relationship between remotely-sensed vegetation indices, canopy attributes and plant physiological processes: what vegetation indices can and cannot tell us about the landscape, Sensors-Basel, 8, 2136–2160, doi:10.3390/S8042136, 2008.

Glenn, E. P., Nagler, P. L., and Huete, A. R.: Vegetation index methods for estimating evapotranspiration by remote sensing, Surv. Geophys., 31, 531–555, doi:10.1007/s10712-010-9102-2, 2010.

Hansen, M., DeFries, R., Townshend, J. R., and Sohlberg, R.: Global landcover classification at 1 km spatial resolution using a classification tree approach, Int. J. Remote Sens., 21, 1331–1364, doi:10.1080/014311600210209, 2000.

Heiblum, R. H., Koren, I., and Altaratz, O.: Analyzing coastal precipitation using TRMM observations, Atmos. Chem. Phys., 11, 13201–13217, doi:10.5194/acp-11-13201-2011, 2011.

Huete, A., Didan, K., Miura, T., Rodriguez, E. P., Gao, X., and Ferreira, L. G.: Overview of the radiometric and biophysical performance of the MODIS vegetation indices, Remote Sens. Environ., 83, 195–213, doi:10.1016/S0034-4257(02)00096-2, 2002.

Knox, R., Bisht, G., Wang, J. F., and Bras, R.: Precipitation variability over the forest-to-nonforest transition in southwestern Amazonia, J. Climate, 24, 2368–2377, doi:10.1175/2010jcli3815.1, 2011.

Koren, I., Kaufman, Y. J., Remer, L. A., and Martins, J. V.: Measurement of the effect of Amazon smoke on inhibition of cloud formation, Science, 303, 1342–1345, doi:10.1126/science.1089424, 2004.

Koren, I., Martins, J. V., Remer, L. A., and Afargan, H.: Smoke invigoration vs. inhibition of clouds over the Amazon, Science, 321, 946–949, doi:10.1126/science.1159185, 2008.

Lewis, S. L., Brando, P. M., Phillips, O. L., van der Heijden, G. M., and Nepstad, D.: The 2010 Amazon drought, Science, 331, 554, doi:10.1126/science.1200807, 2011.

ACPD
13, 30013–30037, 2013

Malda, D., Vilà-Guerau de Arellano, J., van den Berg, W. D., and Zuurendonk, I. W.: The role of atmospheric boundary layer-surface interactions on the development of coastal fronts, Ann. Geophys., 25, 341–360, doi:10.5194/angeo-25-341-2007, 2007.

Martins, J. V., Tanre, D., Remer, L., Kaufman, Y., Mattoo, S., and Levy, R.: MODIS Cloud screening for remote sensing of aerosols over oceans using spatial variability, Geophys. Res. Lett., 29, 8009, doi:10.1029/2001gl013252, 2002.

Mu, Q., Heinsch, F. A., Zhao, M., and Running, S. W.: Development of a global evapotranspiration algorithm based on MODIS and global meteorology data, Remote Sens. Environ., 111, 519–536, doi:10.1016/j.rse.2007.04.015, 2007.

Nagler, P. L., Scott, R. L., Westenburg, C., Cleverly, J. R., Glenn, E. P., and Huete, A. R.: Evapotranspiration on western US rivers estimated using the Enhanced Vegetation Index from MODIS and data from eddy covariance and Bowen ratio flux towers, Remote Sens. Environ., 97, 337–351, doi:10.1016/j.rse.2005.05.011, 2005.

Nair, U. S., Lawton, R. O., Welch, R. M., and Pielke Sr., R. A.: Impact of land use on Costa Rican tropical montane cloud forests: sensitivity of orographic cloud formation to deforestation in the plains, J. Geophys. Res., 111, D02108, doi:10.1029/2005JD006096, 2003.

Nobre, C. A., Mattos, L. F., Dereczynski, C. P., Tarasova, T. A., and Trosnikov, I. V.: Overview of atmospheric conditions during the Smoke, Clouds, and Radiation – Brazil (SCAR-B) field experiment, J. Geophys. Res.-Atmos., 103, 31809–31820, doi:10.1029/98jd00992, 1998.

Parrish, D. F. and Derber, J. C.: The National Meteorological Center's spectral statistical-interpolation analysis system, Mon. Weather Rev., 120, 1747–1763, doi:10.1175/1520-0493(1992)120<1747:TNMCSS>2.0.CO;2, 1992.

Pielke Sr., R. A., Pitman, A., Niyogi, D., Mahmood, R., McAlpine, C., Hossain, F., Goldewijk, K. K., Nair, U., Betts, R., and Fall, S.: Land use/landcover changes and climate: modeling analysis and observational evidence, Wiley Interdisciplinary Reviews: Climate Change, 2, 828–850, doi:10.1002/wcc.144, 2011.

Rabin, R. M., Stadler, S., Wetzel, P. J., Stensrud, D. J., and Gregory, M.: Observed Effects of Landscape Variability on Convective Clouds, B. Am. Meteorol. Soc., 71, 272–280, doi:10.1175/1520-0477(1990)071<0272:Oeolvo>2.0.Co;2, 1990.

Ramos da Silva, R., Gandu, A. W., Sá, L. D. A., and Silva Dias, M. A. F.: Cloud streets and land–water interactions in the Amazon, Biogeochemistry, 105, 201–211, doi:10.1007/s10533-011-9580-4, 2011.

ACPD
13, 30013–30037, 2013

Ray, D. K., Nair, U. S., Welch, R. M., Han, Q. Y., Zeng, J., Su, W. Y., Kikuchi, T., and Lyons, T. J.: Effects of land use in southwest Australia: 1. observations of cumulus cloudiness and energy fluxes, J. Geophys. Res.-Atmos., 108, 4414, doi:10.1029/2002jd002654, 2003.

Remer, L. A., Kaufman, Y. J., Tanre, D., Mattoo, S., Chu, D. A., Martins, J. V., Li, R. R., Ichoku, C., Levy, R. C., Kleidman, R. G., Eck, T. F., Vermote, E., and Holben, B. N.: The MODIS aerosol algorithm, products, and validation, J. Atmos. Sci., 62, 947–973, doi:10.1175/Jas3385.1, 2005.

Running, S. W., Justice, C. O., Salomonson, V., Hall, D., Barker, J., Kaufmann, Y. J., Strahler, A. H., Huete, A. R., Muller, J. P., Vanderbilt, V., Wan, Z. M., Teillet, P., and Carneggie, D.: Terrestrial remote-sensing science and algorithms planned for Eos Modis, Int. J. Remote Sens., 15, 3587–3620, doi:10.1080/01431169408954346, 1994.

Saha, S., Nadiga, S., Thiaw, C., Wang, J., Wang, W., Zhang, Q., Van den Dool, H. M., Pan, H. L., Moorthi, S., Behringer, D., Stokes, D., Pena, M., Lord, S., White, G., Ebisuzaki, W., Peng, P., and Xie, P.: The NCEP climate forecast system, J. Climate, 19, 3483–3517, doi:10.1175/Jcli3812.1, 2006.

Salomonson, V. V., Barnes, W. L., Maymon, P. W., Montgomery, H. E., and Ostrow, H.: Modis – advanced facility instrument for studies of the Earth as a system, IEEE T. Geosci. Remote, 27, 145–153, doi:10.1109/36.20292, 1989.

Souza, E. P., Renno, N. O., and Dias, M. A. F. S.: Convective circulations induced by surface heterogeneities, J. Atmos. Sci., 57, 2915–2922, doi:10.1175/1520-0469(2000)057<2915:Ccibsh>2.0.Co;2, 2000.

Ten Hoeve, J., Remer, L., Correia, A., and Jacobson, M.: Recent shift from forest to savanna burning in the Amazon Basin observed by satellite, Environ. Res. Lett., 7, 024020, doi:10.1088/1748–9326/7/2/024020, 2012.

Wang, J., Chagnon, F. J., Williams, E. R., Betts, A. K., Renno, N. O., Machado, L. A., Bisht, G., Knox, R., and Bras, R. L.: Impact of deforestation in the Amazon basin on cloud climatology, P. Natl. Acad. Sci. USA, 106, 3670–3674, doi:10.1073/pnas.0810156106, 2009.

ACPD
13, 30013–30037, 2013

Table 1. Moving window thresholds for Forest Cu (FCu), Deep Convective Cu, and none to spare Cu cloud fields. Thresholds include cloud fraction (CF), mean cloud area ($\overline{A}$), standard deviation of cloud areas (σ_A), mean distance between cloud centroids ($\overline{D}$), and standard deviation of distances (σ_D). Missing data represent thresholds that are not relevant to the analysis.

Parameter →	CF [%]		$\overline{A}$ [km^2]		σ_A [km^2]		$\overline{D}$ [km]		σ_D [km]	
Field Type ↓	Low	High	Low	High	Low	High	Low	High	Low	High
Forest Cumulus	0.15	0.4	1.5	8	1.5	12.5	1.8	3.2	0.6	1.3
Sparse	0	0.1	0	3	0	3	–	–	–	–
Deep Convective	0.6	1	50	–	–	–	–	–	–	–

ACPD
13, 30013–30037, 2013

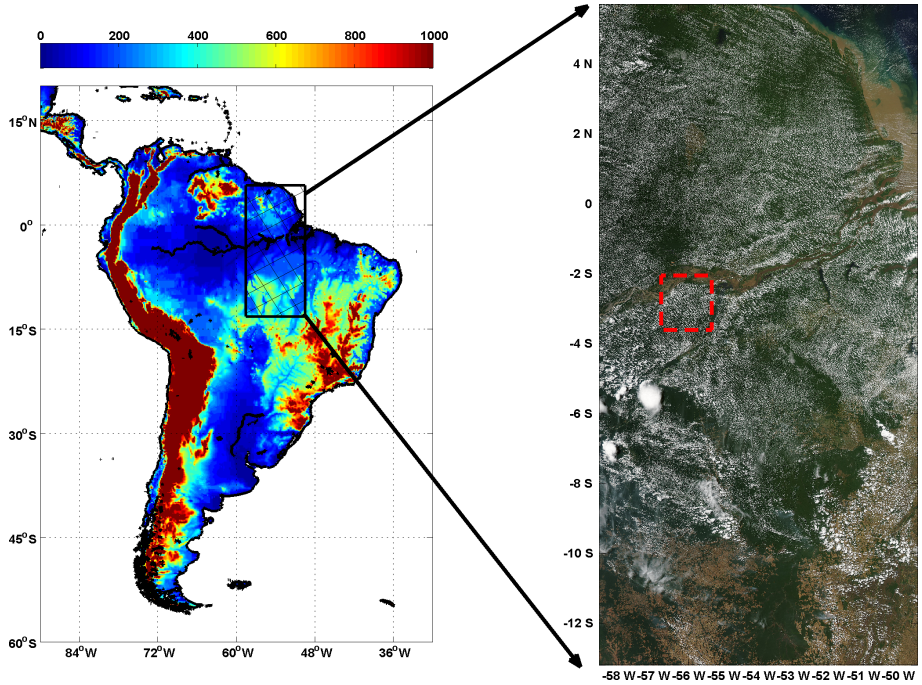

Fig. 1. Left: South America topographic map (note that the color bar is capped at 1000 m) and study region indicated by cross hatched box. Map based on ETOPO1 1-arc minute global relief model dataset (Amante and Eakins, 2009). Right: Typical Forest Cumulus (FCu) fields over the Amazon basin study region. GeoTIFF image taken from MODIS Rapid Response USDA Foreign Agricultural Service (FAS) subsets. Dashed red box indicates the area magnified in Fig. 2. Image corresponds to 1 September 2011, 13:30 local time. The Amazon River and its tributaries seem to inhibit all types of cloud formation.

ACPD
13, 30013–30037, 2013

Fig. 2. Magnified view of Forest Cumulus (FCu) cloud fields (subset of Fig. 1). Note the linear patterns in which the FCu organize. The scale of the box is 150 km × 175 km.

ACPD
13, 30013–30037, 2013

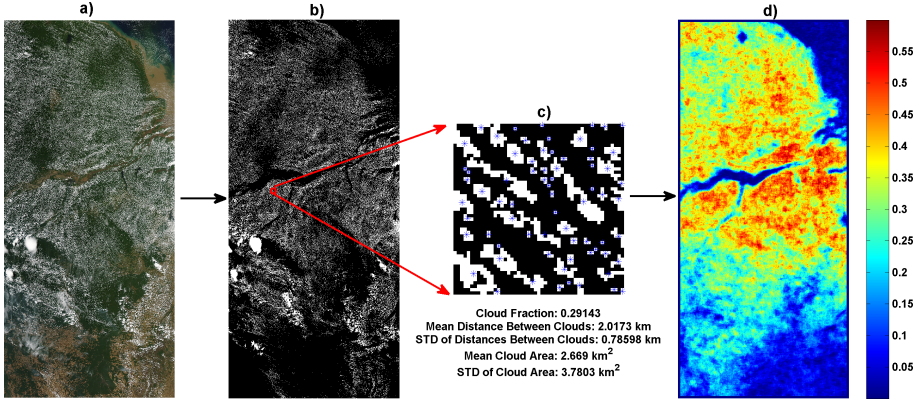

Fig. 3. Summary of FCu field detection algorithm. **(a)** Corresponding true color geoTIFF image from Fig. 1. **(b)** Cloud mask of true color image; the red box represents a 25.5 km × 25.5 km moving window. **(c)** Zoom of the moving window. Blue asterisks indicate the centroids of individual clouds. Selected statistics of windows are listed below the panel. In this case the cloud field within the window passed the FCu field thresholds listed in Table 1. **(d)** Final product of algorithm, probability (0–1) of observing FCu field (pFCu) on a given day during J-A-S 2011.

ACPD
13, 30013–30037, 2013

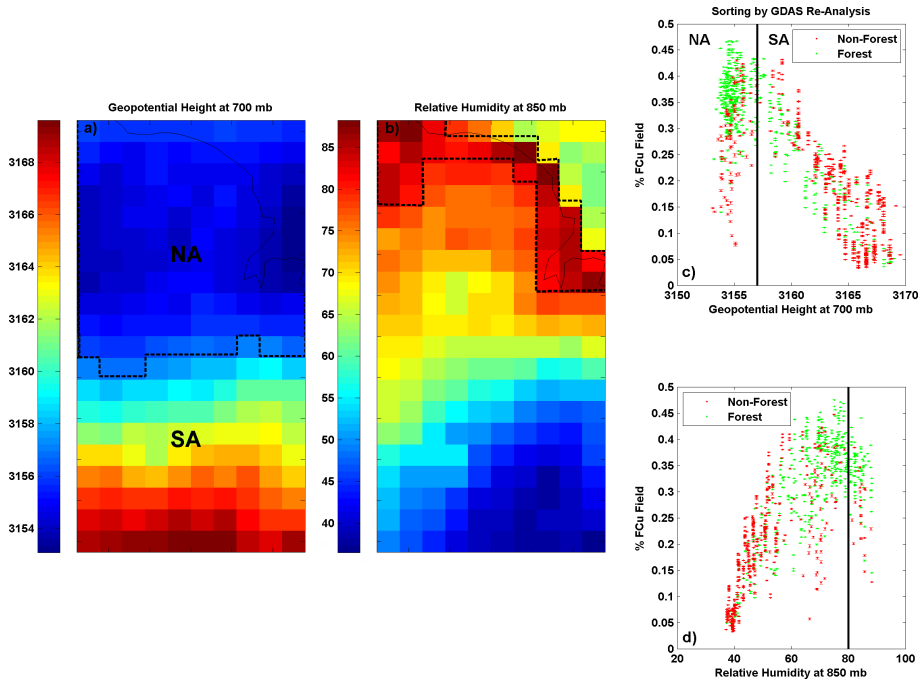

Fig. 4. Meteorological setting (based on GDAS reanalysis data) in the Amazon during J-A-S and the effects on pFCu over forest and non-forest landcovers. **(a)** Geopotential Height (HGT) [m] at 700 hPa pressure level; the dashed line represents the border between NA and SA regions. **(b)** Relative Humidity (RH) [%] at 850 hPa; high RH areas enclosed within the dashed line are excluded from further analyses. **(c)** Chance of observing FCu field as a function of HGT at 700 hPa. Data is sorted into 500 bins, 11 484, 2808 counts per bin for forest and non-forest, respectively. Black line represents HGT separation between NA and SA regions. **(d)** Same as **(c)**, but for RH at 850 hPa. Data above RH = 80 % (black line in panel) is excluded from analyses in this work.

ACPD
13, 30013–30037, 2013

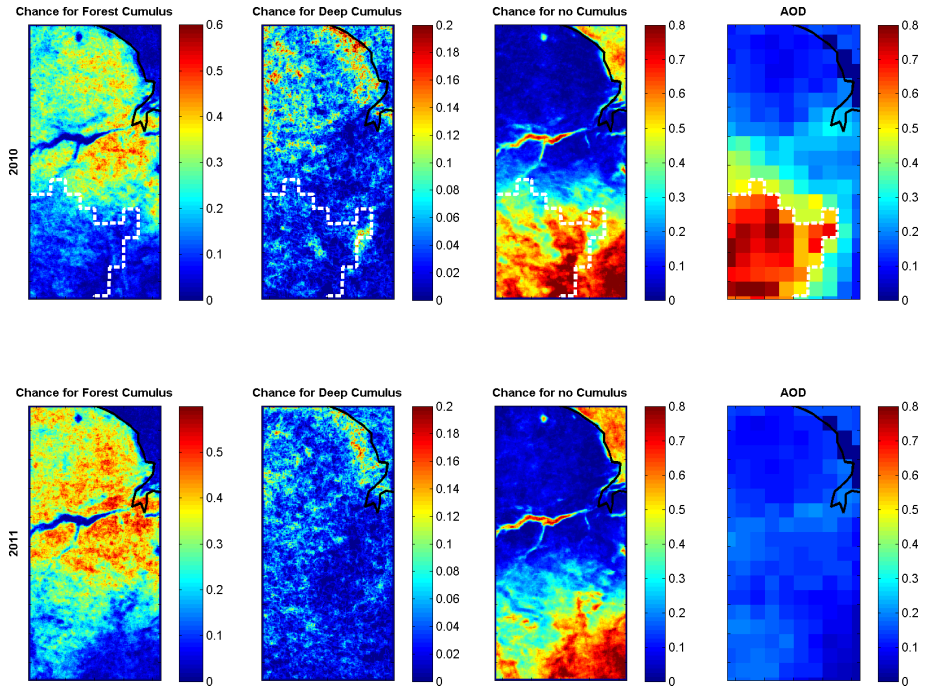

Fig. 5. Cloud field statistics and AOD during J-A-S for 2010 (upper panels) and 2011 (lower panels). Panels include (from left to right) chance for FCu field, chance for deep convective cumulus field, chance for sparse to none cumulus field, and mean AOD taken from Giovanni online data system. White dashed contours in upper panels indicate AOD > 0.5 region. The effects of high AOD during 2010 are apparent in all types of cloud fields, where the high AOD plume clearly inhibits FCu fields in southwest Amazon in comparison with 2011. High AOD pixels along the mouth of the Amazon River were discarded as they correspond to a MODIS AOD algorithm artifact in that area due to the sediment-laden waters there.

ACPD
13, 30013–30037, 2013

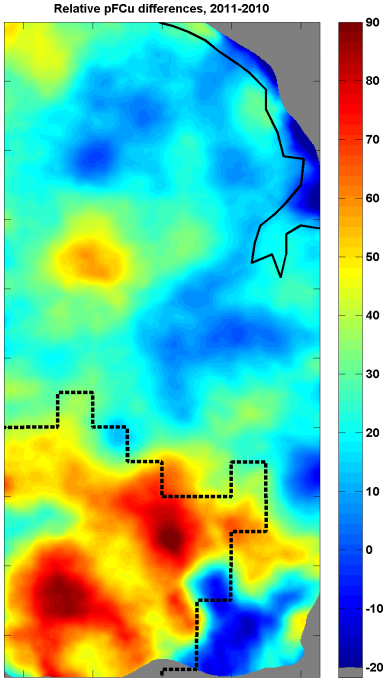

Fig. 6. Relative differences (%) in pFCu between 2011 and 2010. Higher probabilities during 2011 (2010) are represented by red (blue) shades. Black dashed line indicates the high 2010 AOD region in Fig. 5. The largest relative changes (up to 90 %) occur in the region of high AOD. Areas with $\overline{\text{pFCu}} < 0.03$ are discarded.

ACPD
13, 30013–30037, 2013

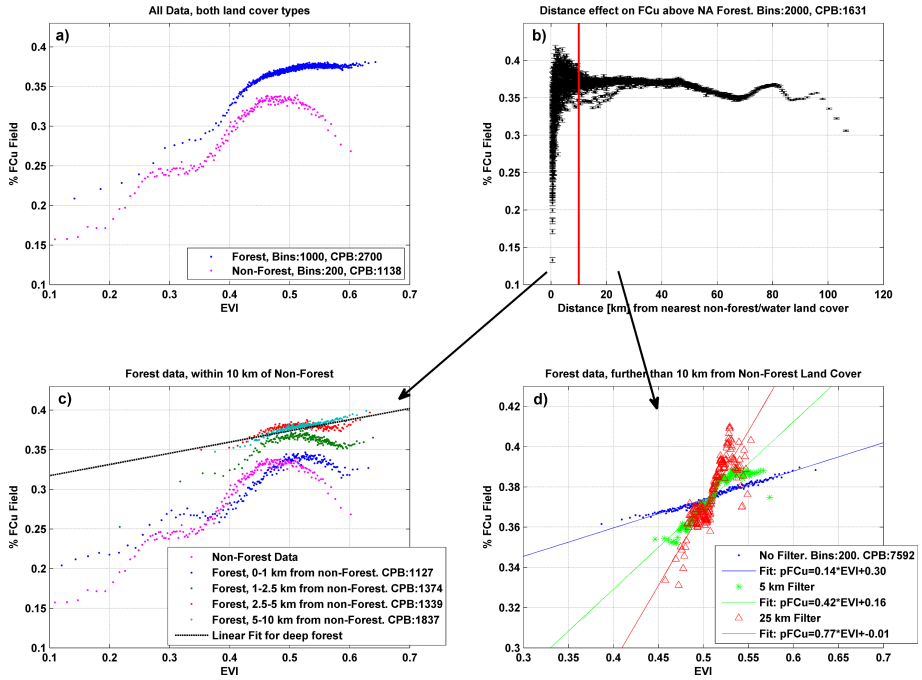

Fig. 7. pFCu field as a function of EVI in the NA region (with RH < 80 %) during J-A-S, 2011. **(a)** All data above forest and non-forest landcover types. Counts per Bin (CPB) appear in panel legend. **(b)** pFCu field over forest landcover as a function of distance (km) from nearest non-forest/water landcover pixel. Data corresponds to NA region (with RH < 80 %). **(c)** Same as **(a)**, but with forest landcover data constrained to within 10 km of other landcover types and sorted into 200 bins. The forest data was divided into four distance subsets (see legend) to illustrate the transition from a non-forest-like dependence to a deep-forest-like dependence. Black dashed line is the linear fit for deep forest EVI dependence seen in **(d)**. **(d)** Same as **(a)**, but only for forest landcover data further than 10 km from other landcover types. Panel includes raw EVI data (blue), and EVI smoothed with a 5 km (red) or 25 km (green) disk filter. Linear fits for all cases added in panel legend.

ACPD
13, 30013–30037, 2013